Design and Experimental Verification of a 0.19 V 53 μW 65 nm CMOS Integrated Supply-Sensing Sensor With a Supply-Insensitive Temperature Sensor and an Inductive-Coupling Transmitter for a Self-Powered Bio-sensing System Using a Biofuel Cell

Atsuki Kobayashi, *Student Member, IEEE*, Kei Ikeda, *Student Member, IEEE*, Yudai Ogawa, Hiroyuki Kai, Matsuhiko Nishizawa, Kazuo Nakazato, *Member, IEEE*, and Kiichi Niitsu, *Member, IEEE*

***Abstract*—In this paper, we present a self-powered bio-sensing system with the capability of proximity inductive-coupling communication for supply sensing and temperature monitoring. The proposed bio-sensing system includes a biofuel cell as a power source and a sensing frontend that is associated with the CMOS integrated supply-sensing sensor. The sensor consists of a digital-based gate leakage timer, a supply-insensitive time-domain temperature sensor, and a current-driven inductive-coupling transmitter and achieves low-voltage operation. The timer converts the output voltage from a biofuel cell to frequency. The temperature sensor provides a pulse width modulation (PWM) output that is not dependent on the supply voltage, and the associated inductive-coupling transmitter enables proximity communication. A test chip was fabricated in 65 nm CMOS technology and consumed 53 μW with a supply voltage of 190 mV. The low-voltage-friendly design satisfied the performance targets of each integrated sensor without any trimming. The chips allowed us to successfully demonstrate proximity communication with an asynchronous receiver, and the measurement results show the potential for self-powered operation using biofuel cells. The analysis and experimental verification of the system confirmed their robustness.**

***Index Terms*—Bio-sensing, biofuel cell, CMOS, inductive coupling, IoT, self-powered, supply sensing, temperature sensor.**

I. Introduction

APPLICATIONS developed for the Internet of Things (IoT) are starting to play key roles in personal and advanced healthcare owing to the increasing opportunities to access various biological information with the hope that the big data generated from continuous healthcare monitoring will be converted into usable knowledge [1]. For this purpose, wearable sensors have generated considerable recent research interest [2], [3]. Normally, a wearable sensor system for healthcare applications must be comfortable to wear, ensure freedom of movement for the user, and be biocompatible. In addition, wearable systems must be low cost to achieve widespread acceptance in the worldwide market. However, among these objectives, the primary consideration lies in solving several critical technical challenges to derive optimal energy management solutions.

To improve the usability of healthcare IoT applications, the energy sources must be considerably reduced in size. The conservative approach is to design conventional battery operated systems to be low power in order to reduce the frequency of replacement. Then, the systems can employ miniature batteries that have sufficient power density. However, this approach increases the risk when these systems are used in or around the human body. In contrast, alternative approaches have emerged that eliminate the need for conventional batteries, and wireless power transfer systems [4], [5] have demonstrated the feasibility of continuous healthcare monitoring. However, it is difficult to cost reduce these systems because of their complex

Manuscript received February 15, 2017; revised June 6, 2017; accepted July 2, 2017. Date of publication October 23, 2017; date of current version December 29, 2017. This work was supported in part by Japan Science and Technology Agency, Precursory Research for Embryonic Science and Technology (no. JPMJPR15D5), in part by a Grant-in-Aid for Scientific Research (S) (nos. 20226009, 25220906, and 26220801), Grants-in-Aid for Young Scientists (A) (no. 16H06088) from the Ministry of Education, Culture, Sports, Science and Technology of Japan, in part by the Strategic Information and Communications R&D Promotion Programme (nos. 121806006, 152106004) of the Ministry of Internal Affairs and Communications, Japan, in part by TOYOTA RIKEN, in part by Hibi Science Foundation, and in part by The Nitto Foundation. The fabrication of CMOS chips was supported by the VLSI Design and Education Center, University of Tokyo, in collaboration with Synopsys, Inc., and Cadence Design Systems, Inc. This paper was recommended by Associate Editor J. Ohta. *(Corresponding author: Kiichi Niitsu.)*

A. Kobayashi, K. Ikeda, and K. Nakazato are with Nagoya University, Nagoya 464-8603, Japan (e-mail: kobayashi.atsuki@d.mbox.nagoya-u.ac.jp; ikeda.kei@g.mbox.nagoya-u.ac.jp; nakazato@nuee.nagoya-u.ac.jp).

Y. Ogawa was with Tohoku University, Sendai 980-8577, Japan.

H. Kai and M. Nishizawa are with Tohoku University, Sendai 980-8577, Japan (e-mail: kai@biomems.mech.tohoku.ac.jp; nishizawa@biomems.mech.tohoku.ac.jp).

K. Niitsu is with Nagoya University, Nagoya 464-8603, Japan, and also with Precursory Research for Embryonic Science and Technology (PRESTO), Japan Science and Technology Agency, Saitama 332-0012, Japan (e-mail: niitsu@nuee.nagoya-u.ac.jp).

Color versions of one or more of the figures in this paper are available online at http://ieeexplore.ieee.org..

Digital Object Identifier 10.1109/TBCAS.2017.2735447

power management units. In addition, self-powered devices that obtain power from energy harvesting, such as heat, solar light, and vibration, have limitations on their conditions of use [6].

The concept of utilizing the energy in living systems [7] suggests a possible design for other beneficial bio-sensing systems. In particular, biofuel cells [8] can potentially be used to power bio-sensing systems that are in close relationship with the human body. Biofuel cells can convert the chemical energy of biofuels, such as glucose and lactate, to electrical energy and provide power to a healthcare device, and are currently undergoing intensive development for various applications, such as CMOS-process-compatible glucose fuel cells [9], transdermal patches [10], and tattoo-type lactate fuel cells [11]. In addition, biofuel cells are being recognized as a stable, safe, clean, and low-cost energy source. Biofuels, such as glucose and lactate, are abundant in the human body and both are well-known biomolecules used in a variety of healthcare applications, such as diabetes monitoring and tracking fitness levels. In addition, the conversion process of these biofuels does not generate reaction products harmful to the human body.

Numerous research activities in the area of biofuel cells have shown the feasibility of using biofuel cells for power generation and as bio-sensing frontend devices [12]. It has been shown that the output power densities of biofuel cells are dependent on the concentration of the biofuels, and hence the concentration of the biofuels can be determined by measuring the power densities of biofuel cells. However, biofuel cells are temperature-sensitive, and their performance deteriorates over time. These technical challenges associated with biofuel cells are attributed to the performance of the enzyme, used to convert ambient biofuels to electrical energy. The power of biofuel cells decreases, as temperature variation causes the denaturation of the enzyme if the temperature domain exceeds the active condition of the enzyme [13]. In addition, these biofuel cells typically have output voltages of less than 400 mV and low power densities, which are too low for powering traditional analog sensing frontend systems that involve ADCs unless voltage boost converters [7] are integrated or multiple biofuel cells are connected in series [14]. Specifically, the maximum available power of biofuel cells can be obtained at voltages of 200 mV to 400 mV owing to the nonlinear voltage current characteristic, and is limited to the order of μW/cm^2. Thus, the sensing system needs to be low-voltage-friendly, low cost, and temperature-monitored to address the technical challenges of biofuel cells.

To overcome the first two issues, we previously proposed a supply-sensing biosensor platform powered directly by a biofuel cell without supply voltage regulation [15]. The platform could detect the biofuel concentration from the supply voltage for healthcare monitoring. By using the biofuel cell as both the energy source and bio-sensing frontend, and adopting a supply-sensing scheme that detects the biofuel concentration as the supply voltage from a biofuel cell, the typically required area-hungry power management circuits, dedicated sensing electrodes, and ADCs could be eliminated, thereby avoiding architectural complexity and costly design of the platform. The platform achieved 230 mV operation at the expense of a large current consumption (1.52 mA) due to the power-hungry ring oscillator and inductive-coupling transmitter with zero-threshold-voltage transistors. However, before the platform can be attached to the human skin without causing undue stress, the current consumption must be reduced.

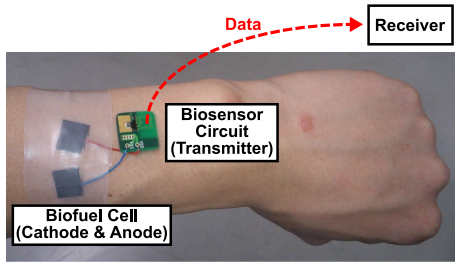

Fig. 1. Proposed bio-sensing system.

This paper presents the design and experimental verification of a self-powered bio-sensing system that uses a biofuel cell for supply sensing and temperature monitoring [16]. The supply-sensing scheme is employed to obtain the concentration of biofuels such as glucose or lactate used in healthcare monitoring. The proposed bio-sensing system detects the output power of biofuel cells that has a relationship with biofuel concentration and converts the supply voltage to a time-domain signal. The system includes a digital-based gate leakage timer, supply-insensitive time-domain temperature sensor, and inductive-coupling link. To calibrate the output of biofuel cells that are subject to changes in temperature, a temperature sensor was implemented. The proposed bio-sensing system, shown in Fig. 1, is self-powered, noninvasive, and facilitates real-time healthcare monitoring. The two black squares in the figure are the cathode and anode, respectively, of the biofuel cell [10], which converts the biofuel of the skin into an electrical power supply for the biosensor circuit. Then, the biosensor circuit transmits the sensed supply voltage and temperature data through the inductive-coupling link to a receiver. The measurements made with a 65 nm CMOS transmitter prototype showed a reduced voltage (190 mV), power (53 μW), and current (280 μA), when compared to the measurements for the previous platform described in [15]. Proximity communication with an asynchronous receiver was also verified. In the following sections, a discussion about the performance of the integrated sensors and the experimental verification is provided to determine the effectiveness of the proposed system.

The remainder of this paper is structured as follows. Section II describes the proposed self-powered bio-sensing system. Section III presents the design of the system prototype. Section IV presents the measurement results of the system. Section V concludes this work.

II. Bio-sensing System

Fig. 2 shows a block diagram of the proposed bio-sensing system consisting of four building blocks: biofuel cells, a digital-based gate leakage timer, a supply-insensitive time-domain temperature sensor, and an inductive-coupling link. On the transmitter side, all circuitry is powered by a biofuel cell without regulation and voltage boosting. Consequently, the circuitry needs to be able to tolerate low-power and low-voltage operation. The

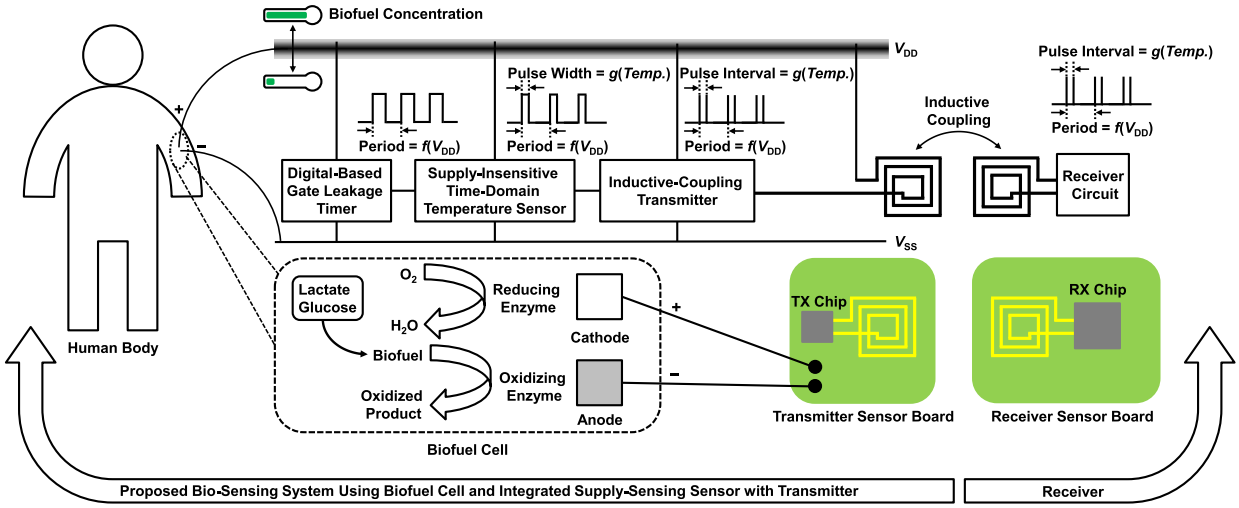

Fig. 2. Block diagram of the proposed bio-sensing system.

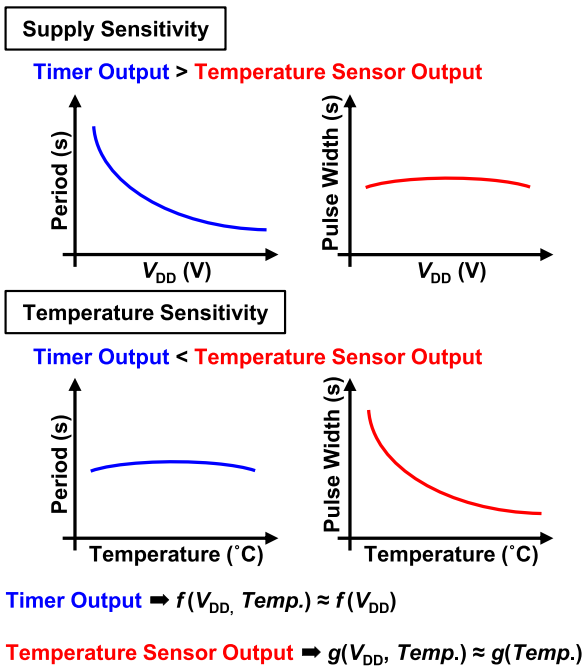

Fig. 3. Required output properties of the timer and temperature sensor.

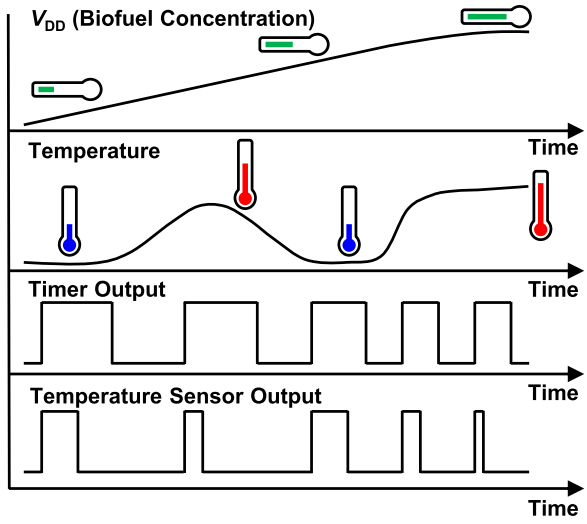

Fig. 4. Operating principle of the proposed bio-sensing system.

digital-based gate leakage timer is used for supply sensing, and converts the supply voltage $V_{\rm DD}$ to the pulse period, which depends on the biofuel concentration. Because the supply-sensing scheme, which is dedicated to unregulated supply voltage operation, is intrinsically unsuitable for pulse-amplitude modulation, pulse-interval modulation (PIM) is employed. The supply-insensitive time-domain temperature sensor, which is used to calibrate the supplied voltage from the biofuel cells, generates a temperature-dependent time-domain output. The inductive-coupling transmitter transmits the signal to the receiver side.

For proper operation, the relationship between the timer and temperature sensor outputs needs to be understood. Fig. 3 shows the required output properties of the timer and temperature sensor. Based on these requirements, it is necessary that these devices be oppositely sensitive to the supply voltage and temperature. The principle of operation of the system when the biofuel concentration and temperature change over time is shown in Fig. 4. The timer converts the supply voltage into a period with inherently temperature-insensitive properties. Subsequently, the time-domain temperature sensor outputs the temperature information with supply-voltage-insensitive properties. The combination of the temperature-insensitive timer and supply-insensitive temperature sensor enables reliable healthcare monitoring through supply sensing using biofuel cells.

A. Digital-Based Gate Leakage Timer

Fig. 5 shows a schematic of the proposed digital-based gate leakage timer, which takes advantage of the fact that bio-sensing does not generally require a rapid sampling rate [17]. The timer, which operates in the kHz range, is employed to sense the supply and then to awaken the temperature sensor and transmitter. To activate the bio-sensing system at a low duty cycle for reducing the overall power consumption, the timer

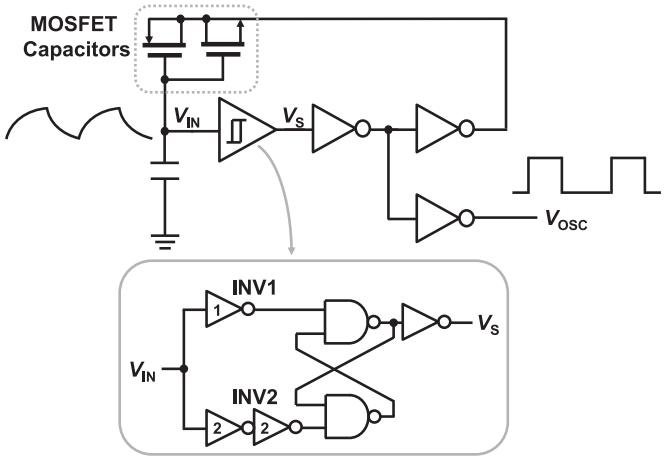

Fig. 5. Schematic of the proposed digital-based gate leakage timer.

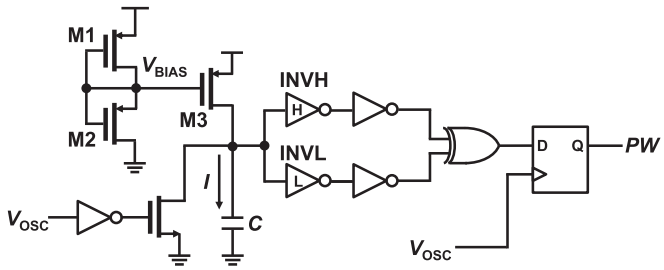

Fig. 6. Schematic of the proposed supply-insensitive time-domain temperature sensor.

must generate a low frequency signal. To minimize the footprint and power consumption, which are the drawbacks of the conventional current source for low power timer circuits, the gate leakage technique was exploited [18] in the design of the low temperature sensitive current source of the timer and to ensure compatibility with the supply voltage reduction. The Schmitt trigger is composed of digital circuitry, which allows operation under the small supply voltage from the biofuel cells. The two inverters, INV1 and INV2, have different transition thresholds and generate a hysteresis characteristic. The temperature sensitivity of the timer mainly depends on the temperature dependency of the gate leakage current of MOSFET capacitors and transition thresholds of the Schmitt trigger. The difference of transition thresholds will increase with the increase in temperature, and that simulation analysis will be explained later in Section III. Thus, the impact of the temperature dependency on the gate leakage current is reduced.

Although other gate-leakage-based timers with higher temperature accuracy have been reported [19], [20], a simple architecture was chosen that could operate with a low supply voltage, ranging approximately from 200 mV to 400 mV, for operation using biofuel cells.

B. Supply-Insensitive Time-Domain Temperature Sensor

Due to the drawbacks of using biofuel cells as the energy source of the system, there were some challenges in designing the temperature sensor. First, the temperature sensor needed to be able to operate from an unregulated low supply voltage with a constrained power budget range of approximately 200 mV to 400 mV for operation using biofuel cells. Second, it was necessary to minimize the supply sensitivity of the output for successful coexistence with the supply-sensing scheme. Fig. 6 shows a schematic of the proposed supply-insensitive time-domain temperature sensor with pulse-width modulation (PWM) output that is capable of low-voltage operation. The PWM output can be used with PIM without difficulty.

Most conventional approaches to temperature sensing utilize the temperature-related voltage of bipolar junction transistors, which offer high resolution but require high power consumption. In contrast, MOSFET-based temperature sensors that use resistor or capacitor for that function [21], [22] are suitable for integrated sensing systems in terms of power consumption. The proposed MOSFET-based temperature sensor can operate in the subthreshold region with limited power from biofuel cells.

Based on the change in temperature, the proposed temperature sensor modulates the pulse width as the output. The width is proportional to the time difference between the times when the voltage across the capacitance *C*, which is charged by current *I*, reaches the logic thresholds of the following two inverters. Therefore, the pulse width *PW* can be expressed as:

$$PW = \frac{C(V_{\mathrm{INVH}} - V_{\mathrm{INVL}})}{I}, \tag{1}$$

where V_{INVH} and V_{INVL} are the logic thresholds of the two inverters INVH and INVL, respectively. Fig. 7 shows the temperature characteristics of each component. The pulse width is inversely proportional to the temperature [see Fig. 7(a)] based on the following mechanism. There are three parts in (1): the capacitance *C*, that is constant for a given temperature and the supply voltage, the difference in the logic threshold of the two inverters, and the current *I*. The latter two are functions of the temperature and supply voltage. By operating the pMOSFET M3 in the subthreshold region, the current *I* can be expressed as:

$$I = \mu C_{\mathrm{ox}} \frac{W}{L} (m-1) V_T^2 \exp\left(\frac{V_{\mathrm{gs}} - V_{\mathrm{th}}}{mV_T}\right) \times \left\{1 - \exp\left(\frac{-V_{\mathrm{ds}}}{V_T}\right)\right\}, \tag{2}$$

where μ is the mobility, C_{ox} is the gate oxide capacitance, m is the subthreshold swing coefficient, and $V_T = kT/q$ is the thermal voltage. The gate of M3 is biased by V_{BIAS}, which is generated as shown in the modified schematic of [23]. The voltage V_{BIAS} can be calculated from the currents I_1 and I_2 through transistors M1 and M2, respectively. Assuming that the voltage V_{BIAS} is far enough above the thermal voltage V_{T}, the subthreshold current becomes independent of the drain-to-

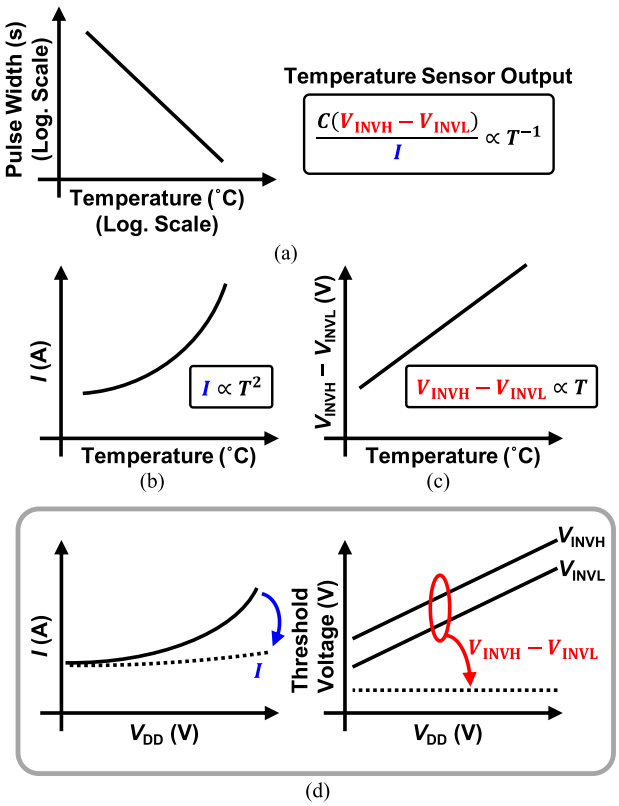

Fig. 7. Temperature characteristics of the (a) pulse width, (b) current *I*, and (c) inverter logic threshold level. (d) Concept of designing the supply insensitive current and the difference in the logic threshold of the two inverters.

source voltage.

$$I_1 = \mu C_{\rm ox} \frac{W_1}{L_1} (m-1) V_T^2 \exp\left(\frac{V_{\rm gs1} - V_{\rm th}}{mV_T}\right) \times \left\{1 - \exp\left(\frac{-V_{\rm ds1}}{V_T}\right)\right\}. \quad (3)$$

$$I_2 = \mu C_{\rm ox} \frac{W_2}{L_2} (m-1) V_T^2 \exp\left(\frac{V_{\rm gs2} - V_{\rm th}}{mV_T}\right) \times \left\{1 - \exp\left(\frac{-V_{\rm ds2}}{V_T}\right)\right\}. \quad (4)$$

$$V_{\rm BIAS} = V_{\rm DD} - mV_T \ln \frac{W_1 L_2}{W_2 L_1}, \quad (5)$$

where $V_{\rm DD}$ is the supply voltage.

If the drain-to-source voltage $|V_{\rm ds}|$ of M3 is sufficiently greater than V_T, the exponential part of $V_{\rm ds}$ can be neglected. Because $V_{\rm BIAS}$ and the threshold voltage $V_{\rm th}$ are proportional to the temperature, and the drain-induced barrier lowering (DIBL) in M3 is designed to be minimized, the current *I* is proportional to V_T^2 [see Fig. 7(b)] and less sensitive to the supply voltage [see Fig. 7(d)]. Then, the current *I* charges capacitance *C* when $V_{\rm OSC}$ is high. The logic thresholds $V_{\rm INV}$ of the subthreshold-operated inverters are known to be proportional to temperature [see Fig. 7(c)].

$$V_{\rm INV} = \frac{V_{\rm DD}}{2} - \frac{mV_T}{2} \ln \frac{I_n}{I_p}, \quad (6)$$

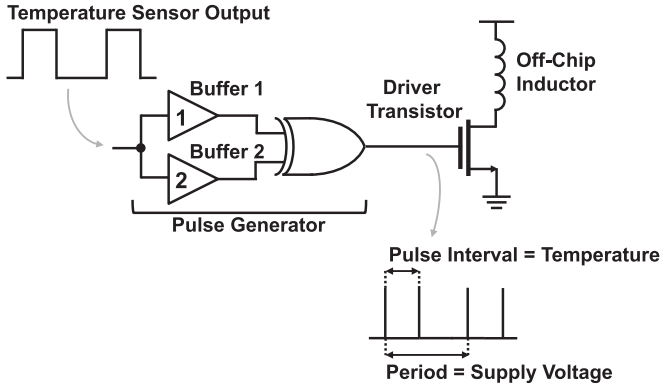

Fig. 8. Schematic of the inductive-coupling transmitter.

where I_n/I_p is the process parameter ratio of the nMOSFET and pMOSFET. By implementing two inverters INVH and INVL with different logic thresholds and subtracting the required time until the capacitor terminal reaches the two logic thresholds of the following normal XOR gate inverter [see Fig. 7(d)], the supply-voltage-independent PWM output can be obtained. The flip-flop is used to remove glitches when the capacitance *C* is discharged.

The threshold voltage difference is determined by the frequency of the timer. Because the temperature sensor becomes active when the timer output is high, the width of the pulse, which is the output of the temperature sensor, should be shorter than the time during which the timer output remains at a high level. If the design does not take this requirement into account, the temperature sensor cannot work properly. In addition, another condition for determining the pulse width of the temperature sensor output is the circuit active area. The pulse width is proportional to the capacitance and is inversely proportional to the current *I*. Therefore, a minimum sized MIM capacitor that is available in the selected 65 nm CMOS technology is implemented. Besides, the size of pMOSFET M3, which is the current source of *I*, should be designed to be minimized with consideration of the DIBL effect. After these steps, the threshold voltage difference will be determined so as not to violate the relationship with the timer output.

C. Inductive-Coupling Link

For low-voltage operation using a biofuel cell, the current-driven inductive-coupling communications method that was proposed in [24] and [25] was adopted. Fig. 8 shows a schematic of the inductive-coupling transmitter in which the input is connected to the temperature sensor output, and the pulse generator is employed to reduce the power in the driver transistor. Meanwhile, the pulse width, which is the output of the temperature sensor, is converted to a pulse interval. Then, the interval between two adjacent pulses contains the temperature information, and the interval between pairs of consecutive pulses contains the supply voltage information. Due to the fact that the frequency of the temperature sensor output follows that of the timer and because of the pulse width to pulse interval modulation, the operational frequency of the transmitter becomes twice as high

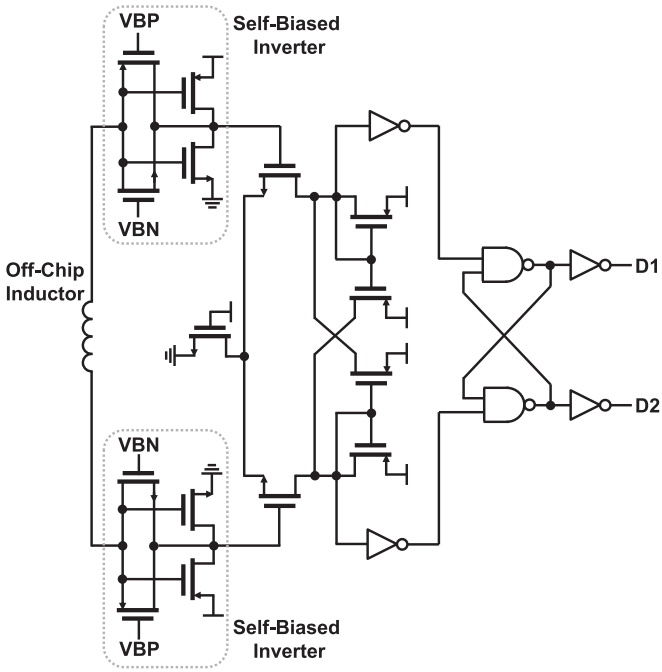

Fig. 9. Schematic of the inductive-coupling receiver.

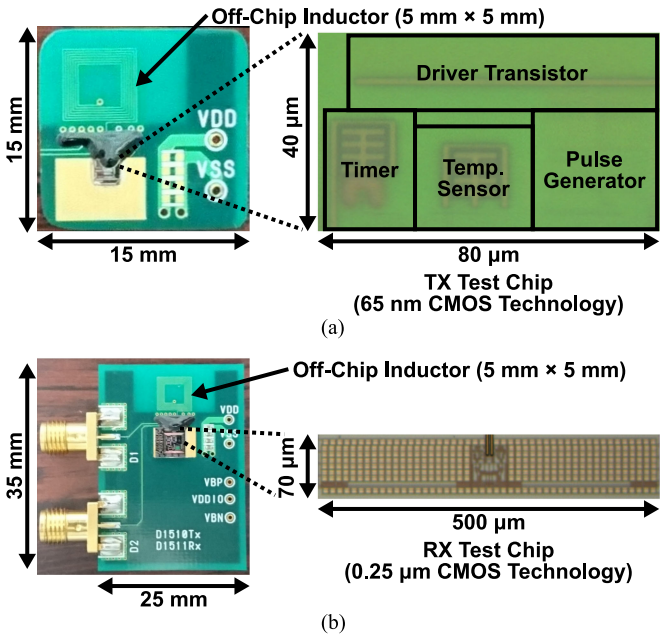

Fig. 10. Microphotographs of the prototype sensor boards and CMOS test chips: (a) transmitter in 65 nm CMOS and (b) receiver in 0.25 μm CMOS.

as that of the timer. In addition, the transmitter should limit the current to less than 1 mA for transmitting the data, considering wearable usage and the supply voltage range of approximately 200–400 mV for operation using biofuel cells.

Asynchronous communications using the inductive-coupling receiver was adopted for PIM signaling. Fig. 9 shows a schematic of the receiver circuit. First, the received voltage of the off-chip inductor is detected by the self-biased inverters. The sensitivity of the receiver circuit can be changed by changing the bias voltages of VBN and VBP. Subsequently, the detected

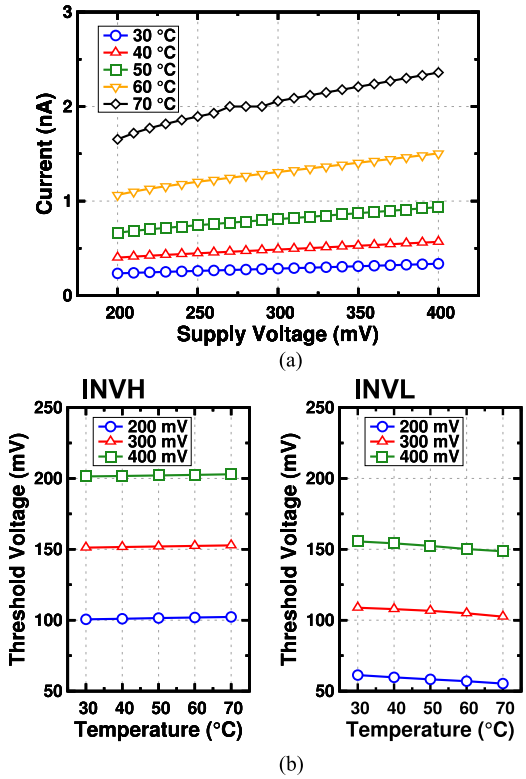

Fig. 11. Simulated results of (a) current I and (b) two inverters, INVH and INVL of the temperature sensor.

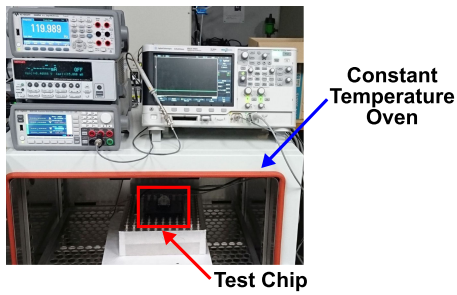

Fig. 12. Experimental setup for measurements of the proposed timer and proposed temperature sensor.

voltage is amplified through the hysteresis comparator. Then, the NAND latch is used to ensure the differential outputs D1 and D2.

III. System Implementation

Prototypes of the sensor boards were fabricated for the design and experimental verification of the proposed system, as shown in Fig. 10. The chips were directly wire-bonded to the printed circuit boards (PCB). Silicon sealing was employed to prevent the wires from being unintentionally disconnected from the contacts. To achieve a longer communication distance, which is the length of the space between the inductor of the inductive-coupling transmitter and that of the receiver, than that in the 3D system integration [24], [25], an off-chip inductor was formed in the PCB. An inductor identical to that of the transmitter was

used in the receiver. The inductance of the off-chip inductor of 380 nH was calculated using the methods in [26].

The test transmitter chip of the proposed system is shown in Fig. 10(a), and was fabricated using 65 nm CMOS technology with an active area of 0.0032 mm^2. The advanced CMOS technology was used because it enabled the low-voltage and low-power operation of the transmitter in a small footprint. In practical applications, the transmitter sensor board can be stacked on top of the biofuel cell, and the occupied area will therefore be determined by that of the biofuel cell.

The capacitors of both the timer and the temperature sensor are sized to be approximately 200 fF. Each occupied area, which is the minimum size available in the process technology, is 0.001 mm^2 (10 μm $\times$ 10 μm). The frequency of the timer is designed not to exceed the kHz range by changing the size of the MOSFET capacitors used as the gate leakage current source. The simulated results of current I and the two inverters, INVH and INVL, are shown in Fig. 11. The current I of the temperature sensor is designed to be supply insensitive, as shown in Fig. 11(a). The difference of transition thresholds is used to generate the output of the temperature sensor and reduce supply sensitivity, and the simulated results are shown in Fig. 11(b). In addition, the characteristic that the difference of transition thresholds increases with the increase in temperature helps to reduce the temperature sensitivity of the timer.

The asynchronous receiver circuit was fabricated with 0.25 μm CMOS technology and had an active area of 0.035 mm^2, as shown in Fig. 10(b). This legacy CMOS technology was selected for cost reasons. In this work, the design of the receiver sensor board was focused on verification of the inductive-coupling communications method, and did not include circuit techniques, such as calibration or statistical processing. The primary focus of this work is designing the low-cost bio-sensing system. It can be achieved with the transmitter powered by the biofuel cell that is low cost for disposable use and the receiver that can be permanently used. Thus, the variations of the transmitter, leading to high cost incurred because of trimming or calibration, can be controlled by the improvements in the receiver.

IV. Measurement

To validate the design of the timer and temperature sensor, the outputs of both the supply and temperature sensor must follow the properties shown in Fig. 3. The characteristics of the test chips of the timer and temperature sensor were measured inside a constant temperature oven. The experimental setup is shown in Fig. 12. The measured samples of the timer and temperature sensor operated correctly.

Fig. 13 shows the measured output frequency across five samples and temperature sensitivity of the timer. The frequency increased with the supply voltage. The measurements revealed that the average frequency was 1.83 kHz at a supply voltage of 200 mV with a standard deviation of 130 Hz (or 6.83%). An almost linear relationship between the frequency and supply voltage was confirmed at room temperature. Keysight 34465A was used to characterize the resolution of the timer

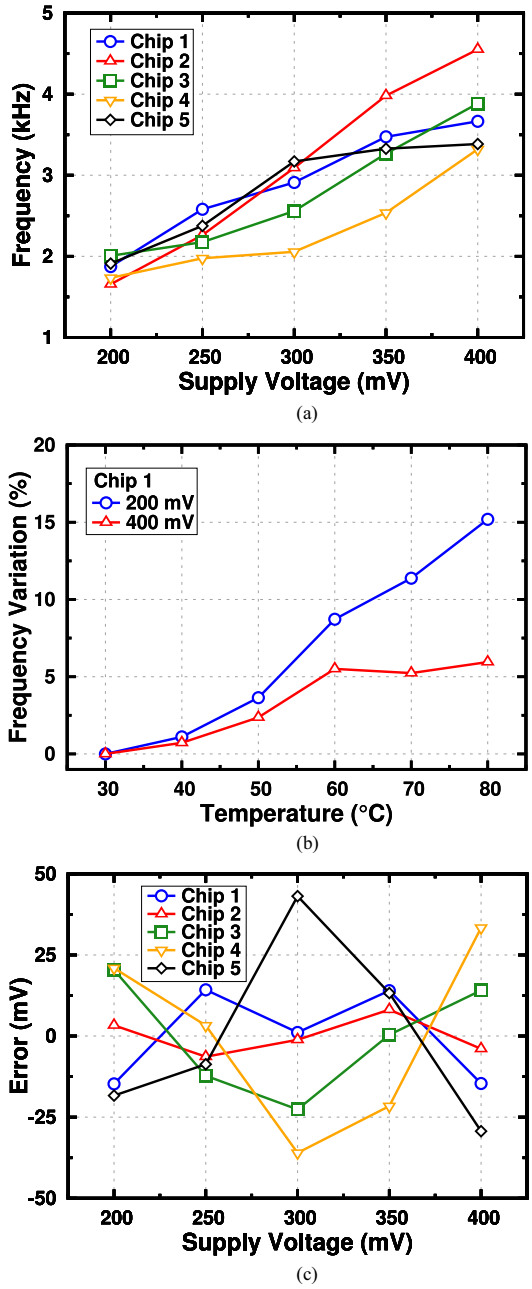

Fig. 13. (a) Measured frequency of the timer as a function of the supply voltage for the five samples at room temperature, (b) measured frequency variation as a function of temperature of Chip 1, and (c) measured linearity of the timer.

(supply-sensing sensor). The resolution was 0.001 mV with the average sensitivity of 5410 ppm/mV over the supply voltage range of 200–400 mV, as shown in Fig. 13(a). On the other hand, from the result of Chip 1, the temperature sensitivities were 3200 ppm/°C and 1330 ppm/°C at supply voltages of 200 mV and 400 mV, respectively, as shown in Fig. 13(b). The frequency variation resulted in a voltage inaccuracy of 31 mV and 24 mV at supply voltages of 200 mV and 400 mV, respectively. The temperature impact on the frequency variation is mainly due to the temperature-related threshold voltages of the two inverters in the Schmitt trigger of the timer. Therefore, the frequency variation of the timer against temperature was reduced at

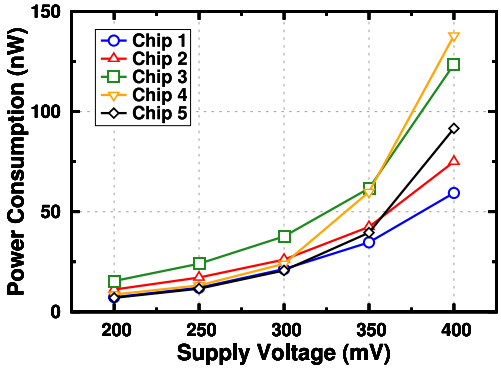

Fig. 14. Measured power consumption of the timer as a function of the supply voltage for the five samples at room temperature.

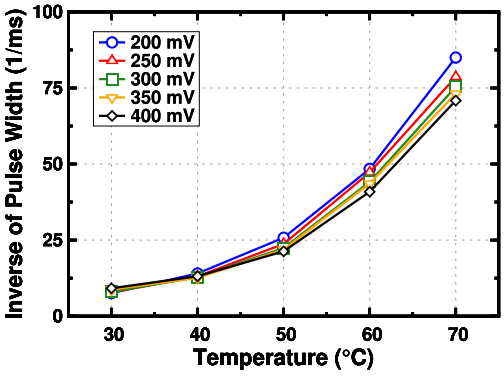

(a)

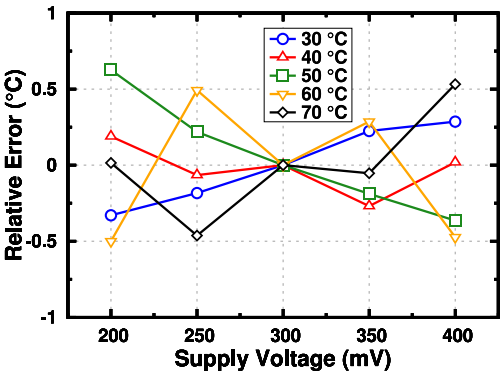

(b)

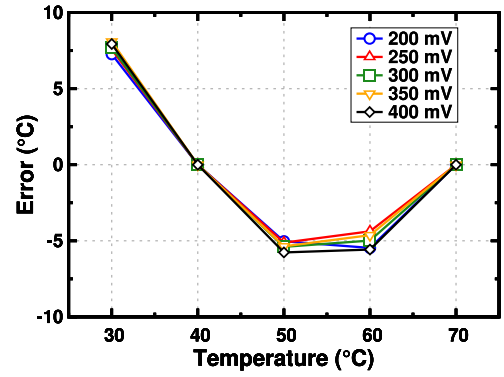

(c)

Fig. 15. (a) Inverse of measured output of the temperature sensor as a function of temperature, (b) measured relative error as a function of the supply voltage, and (c) measured temperature error after two-point calibration.

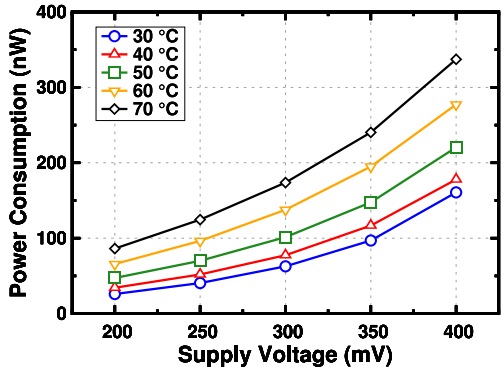

Fig. 16. Measured power consumption of the temperature sensor as a function of the supply voltage at different temperature points.

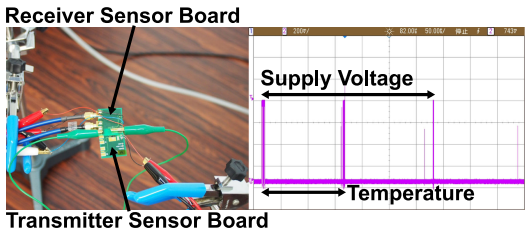

(a) (b)

Fig. 17. Demonstration of inductive-coupling communication: (a) measurement setup and (b) measured result.

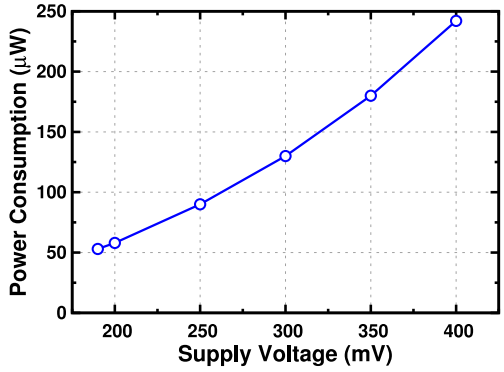

Fig. 18. Measured power consumption of the transmitter as a function of the supply voltage.

the higher supply voltage with the nearly superthreshold region operated digital circuitry in the timer. Fig. 13(c) shows the measured linearity of the timer. The voltage inaccuracy of the timer was within $-36/+43$ mV. Fig. 14 shows the measured power consumption of the timer as a function of the supply voltage. The power consumption of the timer reached a minimum of 7.3 nW at a supply voltage of 200 mV with a standard deviation of 3.1 nW (or 31%). Based on these results, the supply sensitivity and temperature sensitivity are consistent with those outlined in the conceptual design as shown in Fig. 3.

Fig. 15(a) shows the inverse of the measured output of the temperature sensor as a function of the temperature. Another chip sample from the measurement of the design validation for the timer was evaluated. Across a temperature range of

TABLE I
PERFORMANCE SUMMARY AND COMPARISONS TO OTHER WORKS

Supply-Sensing Sensor	This Work	BioCAS 2015 [14]	Angew. Chemie 2013 [11]	Electrochem. Commun. 2014 [27]
Technology	65 nm	0.25 μm	–	–
Type	Using Biofuel Cells	Using Biofuel Cells	Lactate Sensor (Tattoo)	Glucose Sensor (Microneedle)
Supply Voltage	190 mV	230 mV	–	–
Power/Power Density	53 μW	350 μW	$5-70\,\mu\mathrm{W}\cdot\mathrm{cm}^{-2}$	$3-7\,\mu\mathrm{W}\cdot\mathrm{cm}^{-2}$
Temperature Monitoring	Supply-Insensitive Temperature sensor	–	–	–
Wireless	Inductive Coupling	Inductive Coupling	–	–
Area	0.0032 mm^2 (Active Area)	0.0072 mm^2 (Active Area)	18 mm^2 (2 Electrodes)	0.6 mm^2 (6 Needles)

30–70 °C, the approximate inverse proportionality of the pulse width to the temperature was confirmed over the range of the supply voltage from 200 mV to 400 mV. The rate of the output change of the temperature sensor was 2.7 °C/μs. Keysight DSOX2002A was used to characterize the temperature resolution of the temperature sensor output. The temperature resolution of the temperature sensor was measured to be approximately 0.015 °C across a temperature range of 30–70 °C. Across a temperature range of 30–70 °C, the peak-to-peak temperature sensitivity was 255630 ppm/°C and 168210 ppm/°C at supply voltages of 200 mV and 400 mV, respectively. Fig. 15(b) shows the measured relative error in the output of the temperature sensor at different temperature points. The relative error in the supply voltage from 200 mV to 400 mV was mitigated to within $-0.5/+0.6\,^{\circ}\mathrm{C}$, and showed that the peak-to-peak supply sensitivities were 590 ppm/mV and 1150 ppm/mV at 30 °C and 70 °C, respectively. Fig. 15(c) shows the measured temperature error of the temperature sensor after two-point calibration. Across a temperature range of 30–70 °C, the temperature error was $-5.8/+8.1\,^{\circ}\mathrm{C}$. Fig. 16 shows the measured power consumption of the temperature sensor as a function of the supply voltage. The power consumption of the temperature sensor reached a minimum of 25 nW at a supply voltage of 200 mV, at 30 °C (see Fig. 16). The effectiveness of the temperature sensor, which was designed to be supply insensitive, was confirmed.

Fig. 17 demonstrates the inductive-coupling communication method. The off-chip inductors of the transmitter and receiver were placed face to face, as shown in Fig. 17(a), and the communication distance was longer than 50 μm. Fig. 17(b) shows the output waveform of the receiver. Fig. 18 plots the power consumption of the transmitter as a function of the supply voltage. The system power breakdown at a supply voltage of 200 mV was as follows: 0.013%, 0.033%, and 99.954% for the timer, temperature sensor, and inductive-coupling transmitter, respectively. Most of the power of the system was consumed by the inductive-coupling transmitter. Therefore, the size of the driver transistor in the transmitter is decided at the beginning of the design stage for power optimization because the driver transistor size determines the drive current that flows through the off-chip inductor of the transmitter and communication distance with the receiver. In addition, transmitter operation with a supply voltage of 190 mV was confirmed with a magnetic probe. The power consumption was 53 μW. For the condition that the power consumption of the transmitter changes at different temperature, satisfactory transmitter operation can be achieved by increasing the area of the biofuel cell. However, the operating range is limited by the temperature dependence of the biofuel cell [13]. Table I shows the performance summary and comparisons to other supply-sensing sensors. One should note that the comparison of different supply-sensing sensors, [11] and [27], is not straightforward as the approach to bio-sensing is different. However, the proposed system is potentially important to address the temperature dependence of biofuel cells.

There are several limitations in this study. First, the temperature resolution of the proposed temperature sensor was insufficient for practical biomedical applications. However, the architecture of a supply-insensitive temperature sensor is potentially important for bio-sensing using a biofuel cell with supply sensing. In this work, the proposed system is designed to be widely applicable to various biofuel cells. Thus, the temperature sensor resolution should be optimized for the biofuel cells that are determined by the target of bio-sensing. From (1), the capacitance C should be minimized for improving the temperature resolution. Further, the temperature coefficient of the difference in the logic threshold of the two inverters and the current I should be minimized and maximized, respectively.

V. CONCLUSION

In this paper, we proposed a self-powered bio-sensing system that was capable of proximity communication. A digital-based gate leakage timer and a supply-insensitive time-domain temperature sensor were integrated into the bio-sensing system for detecting the supply voltage and temperature. Test chips using 65 nm and 0.25 μm CMOS technology were fabricated for design and experimental verification purposes. The low-voltage-friendly design satisfied the performance targets of the timer and temperature sensor to operate properly without any trimming. The measurement results of the timer show that the average supply sensitivity and minimum temperature sensitivity were 5410 ppm/mV and 1330 ppm/°C, respectively. In contrast to those of the timer, the measurement results of the temperature sensor show that the minimum supply sensitivity

and temperature sensitivity were 590 ppm/mV and 255630 ppm/°C, respectively.

The transmitter test chip in the bio-sensing system was operated at a supply voltage of 190 mV and consumed 53 μW while successfully demonstrating wireless communications with an asynchronous receiver. To operate the transmitter and conduct bio-sensing with biofuel cells successfully, direct connection of the transmitter and the biofuel cell is necessary. To meet this requirement, the transmitter in the proposed system must tolerate low supply voltages and low power densities of biofuel cells. The 190 mV supply can be obtained from a CMOS-compatible glucose biofuel cell (190 mV output) with relatively a large area of the glucose biofuel cell for the required power of the transmitter [9]. Thus, the proposed sensor can be applied to implantable glucose monitoring. In addition, a lactate fuel cell can generate more than 53 μW and the required supply voltage of the transmitter [11]. Thus, the potential for applications requiring self-powered operation using biofuel cells for health monitoring was confirmed.

REFERENCES

[1] J. A. Stankovic, "Research directions for the internet of things," *IEEE Internet Things J.*, vol. 1, no. 1, pp. 3–9, Feb. 2014.

[2] A. Pantelopoulos and N. G. Bourbakis, "A survey on wearable sensor-based systems for health monitoring and prognosis," *IEEE Trans. Syst., Man, Cybern. C, Appl. Rev.*, vol. 40, no. 1, pp. 1–12, Jan. 2010.

[3] G. Matzeu, L. Florea, and D. Diamond, "Advances in wearable chemical sensor design for monitoring biological fluids," *Sens. Actuators B, Chem.*, vol. 211, pp. 403–418, May 2015.

[4] Y. T. Liao, H. Yao, A. Lingley, B. Parviz, and B. P. Otis, "A 3-μW CMOS glucose sensor for wireless contact-lens tear glucose monitoring," *IEEE J. Solid-State Circuits*, vol. 47, no. 1, pp. 335–344, Jan. 2012.

[5] M. M. Ahmadi and G. A. Jullien, "A wireless-implantable microsystem for continuous blood glucose monitoring," *IEEE Trans. Biomed. Circuits Syst.*, vol. 3, no. 3, pp. 169–180, Jun. 2009.

[6] R. J. M. Vullers, R. van Schaijk, I. Doms, C. V. Hoof, and R. Mertens, "Micropower energy harvesting," *Solid-State Electron.*, vol. 53, no. 7, pp. 684–693, Jul. 2009.

[7] S. Bandyopadhyay, P. P. Mercier, A. C. Lysaght, K. M. Stankovic, and A. P. Chandrakasan, "A 1.1 nW energy-harvesting system with 544 pW quiescent power for next-generation implants," *IEEE J. Solid-State Circuits*, vol. 49, no. 12, pp. 2812–2824, Dec. 2014.

[8] R. F. Drake, B. K. Kusserow, S. Messinger, and S. Matsuda, "A tissue implantable fuel cell power supply," *Trans. Amer. Soc. Artif. Internal Organs*, vol. 16, pp. 199–205, Apr. 1970.

[9] B. I. Rapoport, J. T. Kedzierski, and R. Sarpeshkar, "A glucose fuel cell for implantable brain–machine interfaces," *PLOS One*, vol. 7, no. 6, Jun. 2012, Art. no. e38436.

[10] Y. Ogawa *et al.*, "Organic transdermal iontophoresis patch with built-in biofuel cell," *Adv. Healthcare Mater.*, vol. 4, no. 4, pp. 506–510, Mar. 2015.

[11] W. Jia, G. Valdés-Ramírez, A. J. Bandodkar, J. R. Windmiller, and J. Wang, "Epidermal biofuel cells: Energy harvesting from human perspiration," *Angew. Chem. Int. Ed.*, vol. 52, no. 28, pp. 7233–7236, May 2013.

[12] M. Zhou, "Recent progress on the development of biofuel cells for self-powered electrochemical biosensing and logic biosensing: A review," *Electroanalysis*, vol. 27, no. 8, pp. 1786–1810, Jun. 2015.

[13] N. Mano, F. Mao, and A. Heller, "Characteristics of a miniature compartment-less glucose-O_2 biofuel cell and its operation in a living plant," *J. Amer. Chem. Soc.*, vol. 125, no. 21, pp. 6588–6594, Apr. 2003.

[14] K. MacVittie *et al.*, "From "cyborg" lobsters to a pacemaker powered by implantable biofuel cells," *Energy Environ. Sci.*, vol. 6, no. 1, pp. 81–86, Jan. 2013.

[15] K. Niitsu, A. Kobayashi, Y. Ogawa, M. Nishizawa, and K. Nakazato, "An energy-autonomous, disposable, big-data-based supply-sensing biosensor using bio fuel cell and 0.23-V 0.25-μm zero-Vth all-digital CMOS supply-controlled ring oscillator with inductive transmitter," in *Proc. IEEE Biomed. Circuits Syst. Conf.*, Oct. 2015, pp. 595–598.

[16] A. Kobayashi, K. Ikeda, Y. Ogawa, M. Nishizawa, K. Nakazato, and K. Niitsu, "An energy-autonomous bio-sensing system using a biofuel cell and 0.19 V 53 μW 65 nm-CMOS integrated supply-sensing sensor with a supply-insensitive temperature sensor and inductive-coupling transmitter," in *Proc. IEEE Biomed. Circuits .Syst. Conf.*, Oct. 2016, pp. 148–151.

[17] P. P. Mercier, S. Bandyopadhyay, A. C. Lysaght, K. M. Stankovic, and A. P. Chandrakasan, "A sub-nW 2.4 GHz transmitter for low data-rate sensing applications," *IEEE J. Solid-State Circuits*, vol. 49, no. 7, pp. 1463–1474, Jul. 2014.

[18] Y.-S. Lin, D. Sylvester, and D. Blaauw, "A sub-pW timer using gate leakage for ultra low-power sub-Hz monitoring systems," in *Proc. IEEE Custom Integr. Circuits Conf.*, Sep. 2007, pp. 397–400.

[19] Y. Lee, B. Giridhar, Z. Foo, D. Sylvester, and D. B. Blaauw, "A sub-nW multi-stage temperature compensated timer for ultra-low-power sensor nodes," *IEEE J. Solid-State Circuits*, vol. 48, no. 10, pp. 2511–2521, Oct. 2013.

[20] H. Wang and P. P. Mercier, "A reference-free capacitive-discharging oscillator architecture consuming 44.4 pW/75.6 nW at 2.8 Hz/6.4 kHz," *IEEE J. Solid-State Circuits*, vol. 51, no. 6, pp. 1423–1435, Jun. 2016.

[21] M. K. Law, A. Bermak, and H. C. Luong, "A sub-μW embedded CMOS temperature sensor for RFID food monitoring application," *IEEE J. Solid-State Circuits*, vol. 45, no. 6, pp. 1246–1255, Jun. 2010.

[22] S. Jeong, Z. Foo, Y. Lee, J.-Y. Sim, D. Blaauw, and D. Sylvester, "A fully-integrated 71 nW CMOS temperature sensor for low power wireless sensor nodes," *IEEE J. Solid-State Circuits*, vol. 49, no. 8, pp. 1682–1693, Aug. 2014.

[23] M. Seok, G. Kim, D. Blaauw, and D. Sylvester, "A portable 2-transistor picowatt temperature-compensated voltage reference operating at 0.5 V," *IEEE J. Solid-State Circuits*, vol. 47, no. 10, pp. 2534–2545, Oct. 2012.

[24] K. Niitsu *et al.*, "An inductive-coupling link for 3D integration of a 90nm CMOS processor and a 65 nm CMOS SRAM," in *Proc. IEEE Int. Solid-State Circuits Conf.*, Feb. 2009, pp. 480–481.

[25] N. Miura, D. Mizoguchi, T. Sakurai, and T. Kuroda, "Analysis and design of inductive coupling and transceiver circuit for inductive inter-chip wireless superconnect," *IEEE J. Solid-State Circuits*, vol. 40, no. 4, pp. 829–837, Apr. 2005.

[26] S. S. Mohan, M. M. Hershenson, S. P. Boyd, and T. H. Lee, "Simple accurate expressions for planar spiral inductances," *IEEE J. Solid-State Circuits*, vol. 34, no. 10, pp. 1419–1424, Oct. 1999.

[27] G. Valdés-Ramírez *et al.*, "Microneedle-based self-powered glucose sensor," *Electrochem. Commun.*, vol. 47, pp. 58–62, Oct. 2014.

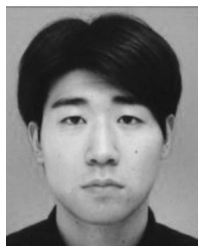

Atsuki Kobayashi (S'16) was born in Yamanashi, Japan, in 1993. He received the B.S. degree in electrical engineering and computer science from Nagoya University, Nagoya, Japan, in 2016, where he is working toward the M.S. degree. His research activity is focused on mixed-signal CMOS integrated circuits for biomedical applications.

Kei Ikeda (S'16) was born in Japan in 1992. He received the B.S. degree in electrical engineering and computer science from Nagoya University, Nagoya, Japan, in 2016, where he is working toward the M.S. degree. His research activity is focused on mixed-signal CMOS integrated circuits for biomedical applications.

Yudai Ogawa was born in Japan in 1988. He received the B.S. degree from Kumamoto University, Kumamoto, Japan, in 2011, and the M.S. and Ph.D. degrees from Tohoku University, Sendai, Japan, in 2013 and 2016, respectively, all in mechanical engineering. His current research interests include biofuel cells, enzyme electrodes, flexible electronics, stretchable electronics, carbon nanomaterials, and cell engineering.

Hiroyuki Kai was born in Japan in 1984. He received the B.Eng. and M.Eng. degrees in chemistry and biotechnology from the University of Tokyo in 2006 and 2008, respectively, and the Ph.D. degree in chemistry from the University of California, Berkeley, in 2015. His research interests include soft, wearable electronics and sensors based on organic and materials chemistry.

Matsuhiko Nishizawa was born in 1965. He received the B.S., M.S., and Ph.D. degrees in applied chemistry from Tohoku University, Japan. From 1995, he was a Research Assistant at Osaka University, and moved to Tohoku University in 1997. Since 2003, he has been a Professor in the Department of Biorobotics, Tohoku University. His main concern is BioMEMS technology including the biological batteries and biocompatible hydrogel electrodes, and its application in medical and healthcare fields. Dr. Nishizawa was awarded the 2000 Young Researcher Award from the Chemical Society of Japan, the 2000 Young Researcher Award from the Electrochemical Society of Japan, and the 2016 Academic Award from the Chemical Society of Japan.

Kazuo Nakazato (M'16) was born in Japan on October 18, 1952. He received the B.S., M.S., and Ph.D. degrees in physics from the University of Tokyo in 1975, 1977, and 1980, respectively. In 1981, he joined the Central Research Laboratory, Hitachi Ltd., Tokyo, working on high-speed silicon self-aligned bipolar devices SICOS (sidewall base contact structure), which were adopted in main frame computer Hitachi M-880/420. In 1989, he moved to Hitachi Cambridge Laboratory, Hitachi Europe, Ltd., Cambridge, England, as a Senior Researcher and a Laboratory Manager, working on experimental and theoretical study of quantum electron transport in semiconductor nanostructures, including single-electron memory. Since 2004, he has been a Professor of intelligent device in the Department of Electrical Engineering and Computer Science, Graduate School of Engineering, Nagoya University, Japan. His main concerns are BioCMOS technology, single molecule-CMOS hybrid devices, and CMOS analog circuits for integrated sensors.

Kiichi Niitsu (S'05–M'10) was born in Japan in 1983. He received the B.S. (summa cum laude), M.S., and Ph.D. degrees in electrical engineering from Keio University, Yokohama, Japan, in 2006, 2008, and 2010, respectively. From 2010, he was an Assistant Professor at Gunma University, Kiryu, Japan. Since 2012, he has been a Lecturer at Nagoya University, Nagoya, Japan. Since 2015, he has been serving concurrently as a Precursory Research for Embryonic Science and Technology (PRESTO) Researcher, Japan Science and Technology Agency (JST). His current research interest lies in the low-power and high-speed technologies of analog and digital VLSI circuits for biomedical application. Dr. Niitsu is a member of the Institute of Electronics, Information and Communication Engineers (IEICE) of Japan, and the Japan Society of Applied Physics (JSAP). From 2008 to 2010, he was a Research Fellow of the Japan Society for the Promotion of Science (JSPS), a Research Assistant of the Global Center of Excellence (GCOE) Program at Keio University, and a Collaboration Researcher of the Keio Advanced Research Center (KARC). He was awarded the 2006 KEIO KOUGAKUKAI Award, the 2007 INOSE Science Promotion Award, the 2008 IEEE SSCS Japan Chapter Young Researcher Award, and the 2009 IEEE SSCS Japan Chapter Academic Research Award both from IEEE Solid-State Circuits Society Japan Chapter, the 2008 FUJIWARA Award from the FUJIWARA foundation, 2011 YASUJIRO NIWA Outstanding Paper Award, 2011 FUNAI Research Promotion Award, 2011 Ando Incentive Prize for the Study of Electronics, 2011 Ericsson Young Scientist Award, 2012 ASP-DAC University LSI Design Contest Design Award, NF Foundation R&D Encouragement Award, AKASAKI Award from Nagoya University, IEEE Nagoya Section Young Researcher Award, and IEEE Biomedical Circuits and Systems Conference 2016 (BioCAS 2016) Best Paper Award and the Young Scientists' Prize of the Commendation for Science and Technology by the Minister of Education, Culture, Sports, Science and Technology. He has published 47 referred original journal papers, 105 international conference papers, and 3 book chapters including 2 TBioCAS, 5 JSSC, 5 TVLSI, 2 ISSCC, 4 Symp. on VLSI Circuits, 11 BioCAS, 1 ISCAS, 4 A-SSCC. He served as a Technical Committee of IEEE (BioCAS TC), a Review Committee Member of ISCAS 2017 and APCCAS 2014, an Associate Editor of IEICE Transactions on Electronics, an Editorial Committee of *IEICE Transactions on Electronics, Special Section on Analog Circuits and Related SoC Integration Technologies*, and an Editorial Committee of IEICE ESS Fundamental Review.